Soft Matter

www.rsc.org/softmatter

Volume 9 | Number 21 | 11 June 2013 | Pages 5127–5306

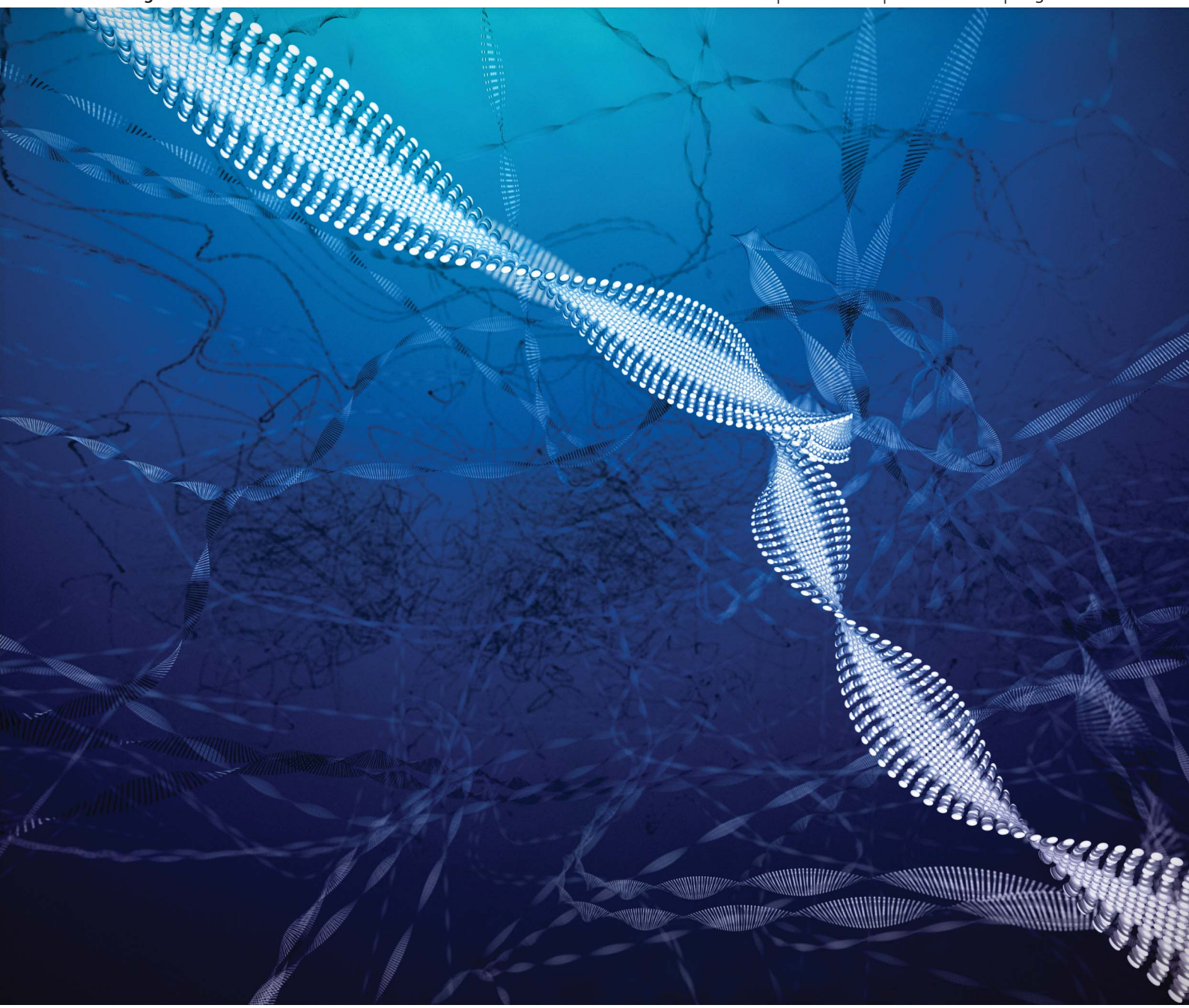

ISSN 1744-683X

RSC Publishing

PAPER

Atsuomi Shundo, Keiji Tanaka *et al.*

Spatial heterogeneity in the sol–gel transition of a supramolecular system

1744-683X(2013)9:21;1-7

Soft Matter

RSC Publishing

PAPER

View Article Online
View Journal | View Issue

Cite this: *Soft Matter*, 2013, **9**, 5166

Spatial heterogeneity in the sol–gel transition of a supramolecular system

David P. Penaloza, Jr.,[a] Atsuomi Shundo,*[a] Keigo Matsumoto,[bc] Masashi Ohno,[c] Katsuaki Miyaji,[c] Masahiro Goto[ad] and Keiji Tanaka*[abe]

Received 21st January 2013
Accepted 14th March 2013

DOI: 10.1039/c3sm50225b

www.rsc.org/softmatter

Heating and then cooling down a dispersion of a peptide amphiphile in water forms hierarchical fibril structures leading to a supramolecular hydrogel. When the gel was physically broken apart by shaking, it transformed into a sol state. After aging it at room temperature for a given time, it returned to the gel state (re-gelation). To obtain a better understanding of such re-gelation processes, we have applied particle tracking to the sol obtained by disrupting the gel, as a function of aging time. The sol was more heterogeneous at the micrometer scale than the initial gel in terms of its viscoelastic properties, and the extent of the heterogeneity in the sol decreased as the re-gelation proceeded. The origin of the heterogeneity could be directly associated with a fibril network confirmed from Fourier-transform infrared spectroscopic, small-angle X-ray scattering and fluorescence microscopic measurements. The particle tracking study using different particle sizes suggested that the characteristic length scale of the heterogeneous network was not larger than 3 μm. This knowledge might be useful for understanding and controlling the gelation, thereby leading to the design and functionalization of soft materials.

Introduction

The physical properties of self-assembled materials rely heavily on the hierarchical structures based on non-covalent bonds formed between the building units.[1] Hence, understanding the relationship between the physical properties and these structures involved in the self-assembly process has been a subject of intensive research over the years.[2] One particular subject of study is the spontaneous self-assembly and network formation involving low-molecular-weight gelators to yield supramolecular hydrogels (SMGs). Attempts to arrive at a better understanding of the gelation behavior have been ongoing.[3] SMGs are soft materials capable of immobilizing a substantially large amount of water within the domains of the three-dimensional networks formed by the entanglement of fibers due to the self-assembly of low-molecular-weight molecules. In contrast to conventional polymeric gels, SMGs are characterized by a reversible transition between sol and gel states. For example, the sol state obtained by mechanically disrupting the gel often returns to the gel state spontaneously (re-gelation).[4] Thus, SMGs are promising candidates for responsive and tunable soft materials such as self-healing materials.[5] To expand the application of SMGs as such materials, it is necessary to understand any correlations between the molecular assembled state, the resulting network structure, and the resulting mechanical properties, as well as the self-assembly mechanism operating during the sol-to-gel transition.

Microrheology encompasses a wide variety of experimental techniques capable of extracting local viscoelastic information.[6] One example of microrheology is a particle tracking method, where viscoelastic information at the micrometer length scale can be accessed by observing the thermal diffusion of embedded particles used as probes. It is a noninvasive approach for investigating the mechanical behavior of fragile materials that are difficult, if not impossible, to characterize using conventional bulk rheological techniques.[7] Also, investigating the behavior of individual particles can provide insights into the existence of any spatial heterogeneity.[8]

In this study, we performed a particle tracking study of the re-gelation process involving a supramolecular gel based on a simple peptide amphiphile that can efficiently gelate water even at a remarkably low concentration.[9] To the best of our knowledge, this is the first study involving the sol-to-gel transition for the re-gelation of a physical gel. Here, we have quantified the changes in the spatial heterogeneity in the system at the micrometer scale based on the diffusion behavior of the probe particles and correlated them to the changes in the molecular assembled state and the network structure as the system transforms from the sol to the gel state.

[a]*Department of Applied Chemistry, Kyushu University, Fukuoka 819-0395, Japan. E-mail: k-tanaka@cstf.kyushu-u.ac.jp; Fax: +81-92-802-2880; Tel: +81-92-802-2878*
[b]*Department of Automotive Science, Kyushu University, Fukuoka 819-0395, Japan*
[c]*Nissan Chemical Industries, Ltd., Tokyo 101-0054, Japan*
[d]*Center for Future Chemistry, Kyushu University, Fukuoka 819-0395, Japan*
[e]*International Institute for Carbon-Neutral Energy Research (WPI-I2CNER), Kyushu University, Fukuoka 819-0395, Japan*

Experimental

Materials

N-Palmitoyl-Gly-Gly-Gly-His trifluoroacetate ($PalG_3H$) was synthesized using a standard Fmoc chemistry procedure.[9] Water, after distillation with an Autostill WG33 (Yamato Scientific Co., Ltd.) and successive deionization with a Milli-Q Lab (Millipore), was used for the hydrogel formation. The specific resistance of the purified water was greater than 18 MΩ cm. For particle tracking measurements, an aqueous dispersion of Fluoresbrite Yellow Green Microspheres – these are polystyrene (PS) particles containing a fluorescence dye – with a concentration of 2.5 wt% was purchased from Polysciences Inc. The particles have a diameter (d) of 1.1 ± 0.03 μm and 3.1 ± 0.09 μm. For the fluorescence spectroscopic and microscopic measurements, sodium 8-anilino-1-naphthalenesulfonate (ANS) purchased from Tokyo Kasei Chemical Co. was used as received. Deuterated water (D_2O) and dimethyl sulfoxide (DMSO-d_6) purchased from MERCK & Co. Inc. and Cambridge Isotope Laboratories, Inc., respectively, were used for the Fourier transform infrared (FT-IR) spectroscopy.

Particle tracking

A 9 mg amount of $PalG_3H$ and 3 μL of the particle dispersion were well-dispersed into 3 mL of pure water by sonication for 10 min. Then, this dispersion was heated to 363 K for 10 min and then was allowed to cool at room temperature. The resulting particle-containing gel was physically broken by shaking with a vortex mixer (Taitec Ltd.) to form the sol. The sol was then placed in a glass bottom dish (MATSUNAMI GLASS Inc. Ltd.) and sealed with a cover glass and vacuum grease. The sample was left undisturbed for 1 h to equilibrate at room temperature prior to the particle tracking observations – this, we regarded as the time-zero for particle measurements after disrupting the gel. Particle tracking measurements were also made using the same sample after various further aging times: 0 h, 24 h, 48 h and 72 h. All measurements were made at room temperature. The setup of the instrument for the particle tracking, as previously reported elsewhere,[8d] is based on an inverted microscope, Nikon ECLIPSE T*i*, with an NA 1.30 oil-immersion objective lens. A halogen lamp was used to illuminate the sample and a charge-coupled device (CCD) camera (DS-Qi1Mc, Nikon Instech Co., Ltd.) was used to acquire images of the particles in the samples at a frame rate of 31 Hz. Imaging software NIS-Elements AR-3.2 (Nikon Instech Co., Ltd.) was employed for the analysis of the trajectory of the particles dispersed in the sample. A total of 20 particles were tracked in each sample with each particle being monitored 10 times.

Fourier-transform infrared spectroscopy

For the Fourier-transform infrared (FT-IR) measurements, 10 mg of $PalG_3H$ was well-dispersed in 1 mL of D_2O by sonication and then this dispersion was kept for 10 min at 363 K, to prepare the gel. The gel, the sol obtained by shaking the gel and the gel obtained by aging the sol for 72 h were used as samples. Also, a DMSO-d_6 solution of $PalG_3H$ solution having the same concentration was prepared to serve as a reference sample. Each of the samples was sandwiched between CaF_2 windows with a 0.5 mm gap. The FT-IR spectra were recorded with a FT/IR-620 spectrometer (JASCO Co.) equipped with a triglycine sulfate (TGS) detector. All spectra were obtained with a resolution of 2 cm^{-1} and 64 scans at 298 K.

Small-angle X-ray scattering measurements

Small-angle X-ray scattering (SAXS) experiments were carried out at the BL40B2 beamline of SPring8 (Japan). The wavelength of the incident X-rays and the sample-to-detector distance were 0.15 nm and 1621 mm, respectively. The gel with a $PalG_3H$ concentration of 0.5 wt% was placed in an aluminum pan and the pan was installed on a sample stage. The scattered X-rays were recorded using a Rigaku R-AXIS IV+++ system (300 × 300 mm imaging plate) for 300 s. By circular averaging of the two-dimensional pattern on the image plate, a one-dimensional scattering profile of the sample was obtained.

Fluorescence spectroscopy and microscopy

A methanol solution of ANS with a concentration of 10^{-3} M was prepared. A 3 μL aliquot of dye solution was added to 3 mL of water, which was placed in a quartz cell having a pathlength of 10 mm. Then, 9 mg of $PalG_3H$ was well-dispersed in the mixture by sonication for 10 min. The dispersion was heated afterwards for 10 min at 363 K. After aging it for 1 hour at 298 K, an ANS-containing gel was obtained. The fluorescence spectra before and after shaking the gel were recorded using an F-4500 Spectrophotometer (Hitachi High-Technologies Co.).

For the fluorescence microscopic observations, an aliquot of the resulting sol containing the ANS dye was placed on a glass slide and covered with a glass coverslip. Fluorescence microscopic images of the sample at various stages of the re-gelation (here, at 0 h, 12 h and 72 h aging times) were obtained using a fluorescence microscope (Nikon ECLIPSE T*i*). A mercury lamp illuminated the sample through an excitation filter housed in a filter block (DAPI, Nikon Instech Co., Ltd.).

Results and discussion

Sol-to-gel transition

Fig. 1 shows the chemical structure of the $PalG_3H$, together with photographs showing the variation in the physical state of the

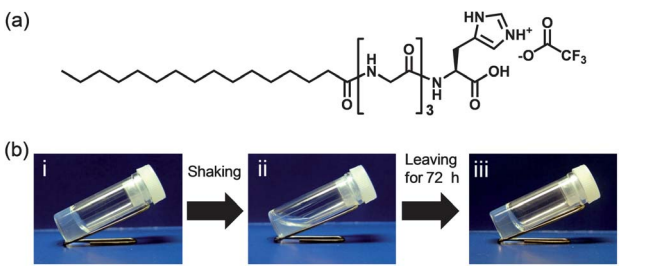

Fig. 1 (a) Chemical structure of the hydrogelator, *N*-palmitoyl-Gly-Gly-Gly-His trifluoroacetate ($PalG_3H$). (b) Photographic image of the $PalG_3H$–water mixture (i) as a gel, (ii) as a sol at 0 h aging and (iii) as a gel at 72 h aging.

mixture of $PalG_3H$ and water. When the gelator, $PalG_3H$, was dissolved in water by heating and then subsequently cooled slowly to room temperature, it formed a hydrogel based on a micelle-like self-assembly to produce a fibrous network.[4d,9] Formation of the hydrogel was confirmed by tilting a vial containing it at an angle, whereupon it did not flow. The gel was then broken by shaking with a vortex mixer, leading to a transparent fluid, namely a sol, which flowed when the vial was tilted. After aging this sol for 72 h, it returned to its gel state. Such a sol-to-gel transition was here subjected to study with the particle tracking measurements.

Particle trajectory profiles

Fig. 2 shows representative two-dimensional trajectories (as x and y displacements) of PS particles ($d = 1.1 \pm 0.03$ μm) embedded in the $PalG_3H$–water mixture at various stages of the sol-to-gel transition (aging times: 0 h, 24 h and 72 h). In all cases, the duration of the trajectories was 3.3 s. Regardless of the aging time, the particles showed erratic and non-directional tracks, indicating thermal diffusion of the particles. In the sol at 0 h aging, the particles diffused around over distances of a few hundred nanometers. However, with an increase in the aging time, the particle motions became more restricted, as shown by the more localized trajectories. This is in good accordance with the macroscopic observation that the fluidity of the sol decreased with increasing aging time (corresponding to the sol-to-gel transition). Here, it should be noted that there was a significant variation in the diffusion distances of each particle especially at the aging time of 0 h. This suggests the possibility of a spatial heterogeneity of the probed environment in the sol. This will be further discussed later.

Mean square displacement

From the trajectories of the individual particles, the mean square displacement, here symbolically represented as $\langle \Delta r^2(\tau) \rangle$, is obtained from the following equation:[10]

$$\langle \Delta r^2(\tau) \rangle = \langle [x(t+\tau) - x(t)]^2 + [y(t+\tau) - y(t)]^2 \rangle \quad (1)$$

where x and y are the time-dependent coordinates of the centroids of the tracked particles, τ is the lag time, and the angular brackets indicate an average over many starting times for the ensemble of particles. The mean square displacement quantitatively measures the average distance travelled by the particles at time τ. Using the slope of the double logarithmic plot of the $\langle \Delta r^2(\tau) \rangle$ against τ, the type of diffusion of the probe particles can be found. For a slope of 1, that is, $\langle \Delta r^2(\tau) \rangle$ linearly scales with τ, the diffusion behavior of the particles is based on a random walk model, assuming that the microenvironment probed by the particles is liquid-like.[8d,11] When $\langle \Delta r^2(\tau) \rangle$ grows more slowly than τ (slope < 1), the particles are considered to display a sub-diffusive behavior. This means that the local environment of the particles is not liquid-like, the sub-diffusive behavior of the particles being generally explained by an elastic trapping of the particles within the network structures in the material.[12]

Fig. 3 shows the correlation between $\langle \Delta r^2(\tau) \rangle$ and τ observed for the probe particles embedded in the $PalG_3H$–water mixture at various stages of the sol-to-gel transition (aging times: 0 h, 24 h, 48 h and 72 h). Each solid line was obtained by monitoring the same particle 10 times and then averaging over them. The slope of the hypotenuse of the right angled triangle in the figures corresponds to unity. The slopes of all plots, regardless of the aging time, are less than unity (slope < 1) suggesting that the fibrous network based on the $PalG_3H$ molecules trapped the particles. The broken lines in Fig. 3 represent the mean-averaged $\langle \Delta r^2(\tau) \rangle$ obtained by averaging $\langle \Delta r^2(\tau) \rangle$ over observed 20 particles. With increasing aging time, the slopes of these broken lines decreased. This indicates that the particles are being increasingly trapped within the network structures during the sol-to-gel transition.

Heterogeneity

Using the particle tracking technique, it is also possible to gain an insight into the presence of heterogeneity in the system of interest. In reference to panel (a) of Fig. 2, we have earlier pointed out the possibility of the existence of heterogeneity on the basis of the fact that there is a large variation in the two-dimensional trajectories of the particles embedded in the sol. To assess this, we examined the shape of the probability distribution of the normalized $\langle \Delta r^2(\tau) \rangle$. The normalized $\langle \Delta r^2(\tau) \rangle$ values are determined by normalizing all individual $\langle \Delta r^2(\tau) \rangle$ values with the mean values at τ. A Gaussian distribution, where the distribution shape is symmetric about a central value of 1,

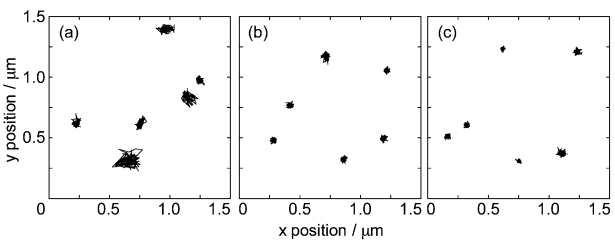

Fig. 2 Representative two-dimensional trajectories of embedded probe particles ($d = 1.1 \pm 0.03$ μm) in the $PalG_3H$–water mixture at various aging times, (a) 0 h, (b) 24 h and (c) 72 h after physically disrupting the gel.

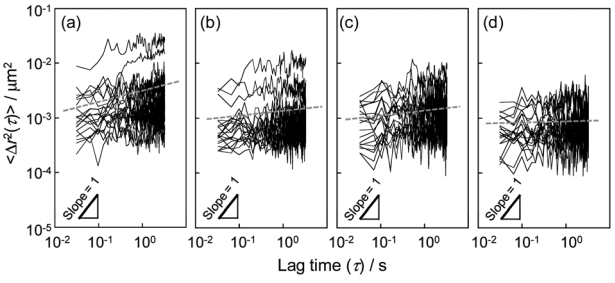

Fig. 3 Double logarithmic plot of $\langle \Delta r^2(\tau) \rangle$ against τ of the probe particles ($d = 1.1 \pm 0.03$ μm) embedded in the $PalG_3H$–water mixture at various aging times, (a) 0 h, (b) 24 h, (c) 48 h and (d) 72 h after physically disrupting the gel. The dotted lines denote the mean-averaged $\langle \Delta r^2(\tau) \rangle$ for all particles.

indicates a homogeneous system. In fact, a homogeneous viscous liquid, such as glycerol, gave a Gaussian distribution.[8d,13] A non-Gaussian distribution of the normalized $\langle \Delta r^2(\tau) \rangle$ suggests that the particles are not in equivalent environments, resulting in the histogram deviating from a Gaussian shape.[8b,14]

Fig. 4 presents the distribution of the normalized $\langle \Delta r^2(\tau) \rangle$ values of the particles in the $PalG_3H$–water mixture at various aging times. In the sol state at 0 h aging, the displacement profiles of the particles produce a non-Gaussian distribution. Upon increasing the aging time, the shape of the distribution changes from being asymmetric to symmetric. Thus, it is likely that the extent of heterogeneity decreases as the sol transforms into the gel. We calculated the non-Gaussian parameter, $\alpha_2(\tau)$, given by

$$\alpha_2(\tau) = \frac{\langle \Delta r^4(\tau) \rangle}{2\langle \Delta r^2(\tau) \rangle^2} - 1 \quad (2)$$

where $\langle \Delta r^4(\tau) \rangle$ is the fourth moment of the particle displacement and $\langle \Delta r^2(\tau) \rangle$ is the second moment of the particle displacement.[15] The $\alpha_2(\tau)$ value is a measure of the deviation from a Gaussian distribution of the particle displacements and therefore reflective of the extent of heterogeneity in the system.[8c,16] Panel (a) of Fig. 5 shows the $\alpha_2(\tau)$ values plotted against τ at various aging times. In the case of the aging times of 24 h, 48 h and 72 h, the $\alpha_2(\tau)$ values were relatively close to zero, independent of the lag time. However, this is not the case for the sol at 0 h aging. The $\alpha_2(\tau)$ values increased with increasing lag time, resulting in larger values at longer lag times. This suggests a more heterogeneous environment as the length scale probed becomes larger.[8c,17] The $\alpha_2(\tau)$ value at the lag time of 1 s was 5.0 and was much higher than that obtained for the gel before shaking ($\alpha_2(\tau) = 0.22$). This indicates that the sol is more heterogeneous than its initial gel state. Importantly, the $\alpha_2(\tau)$ value at $\tau = 1$ decreased with increasing aging time, as shown in Fig. 5(b). Thus, it can be claimed that the sol-to-gel transition process was accompanied by a homogenization of the local environment in the $PalG_3H$–water mixture.

By changing the size of the probe particles, we can qualitatively access information regarding the size scale of the heterogeneity[8d,16b,18] Panel (b) of Fig. 5 includes the results of a parallel experiment employing larger PS particles ($d = 3.1 \pm 0.09$ μm) used as probes. The $\alpha_2(\tau)$ values at $\tau = 1$ were

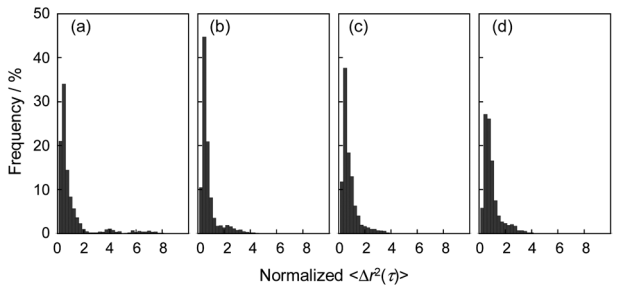

Fig. 4 Probability distribution of the normalized $\langle \Delta r^2(\tau) \rangle$ values of probe particles ($d = 1.1 \pm 0.03$ μm) embedded in the $PalG_3H$–water mixture at various aging times, (a) 0 h, (b) 24 h, (c) 48 h and (d) 72 h after physically disrupting the gel.

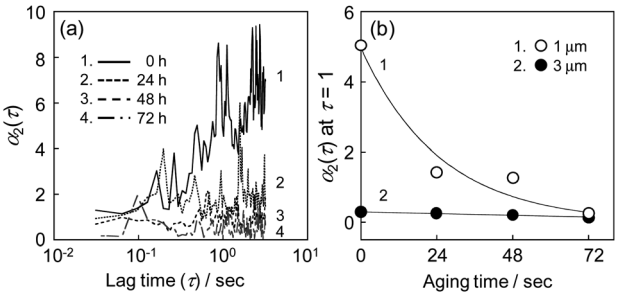

Fig. 5 (a) Non-Gaussian parameter, $\alpha_2(\tau)$, values of probe particles ($d = 1.1 \pm 0.03$ μm) embedded in the $PalG_3H$–water mixture at various aging times, 0 h, 24 h, 48 h and 72 h after physically disrupting the gel. (b) The $\alpha_2(\tau)$ values at $\tau = 1$ s plotted against aging time after physically disrupting the gel which were obtained using two sizes of embedded probe particles ($d = 1.1 \pm 0.03$ μm) and ($d = 3.1 \pm 0.09$ μm).

consistently near zero regardless of the aging time. This indicates that the $PalG_3H$–water mixture behaves as a homogeneous medium on the length scale probed. Although we have tested only two sizes of probe particles, it is worth noting here that the significant difference between the results obtained using these two sizes of probe particles ($d = 1.1 \pm 0.03$ μm *vs.* $d = 3.1 \pm 0.09$ μm) suggests that the smaller size particles may be more sensitive indicators of the length scale of spatial heterogeneity, which we assumed to be less than 1 μm. These results motivated us to examine the fibrous assembly at various length scales and address the origin of the change in the heterogeneity observed during the sol-to-gel transition.

Molecular assembled states

We first examined the structural information available from the $PalG_3H$–water mixtures as a sol and a gel with regard to the assembled state at the molecular level by Fourier-transform infrared (FT-IR) spectroscopic and small-angle X-ray scattering (SAXS) measurements. Fig. 6 shows the FT-IR spectra of $PalG_3H$ in (a) deuterated dimethyl sulfoxide (DMSO-d_6), (b) the initial gel, (c) the sol obtained by shaking the gel and (d) the gel obtained by aging the sol for 72 h. Deuterated solvents were

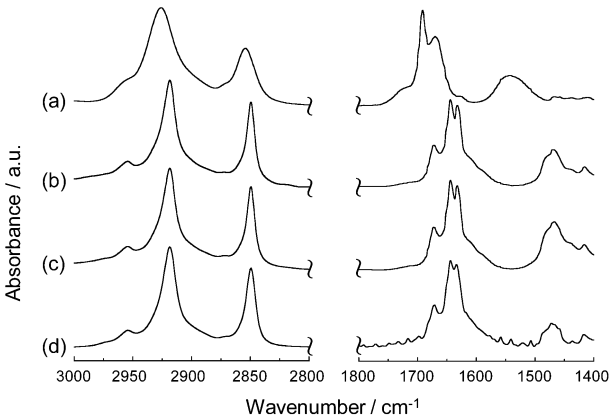

Fig. 6 FT-IR spectra of the $PalG_3H$ mixture (a) as DMSO-d_6 solution (b) as a gel, (c) as a sol at 0 h aging and (d) as a gel at 72 h aging at 298 K.

used for the preparation of all samples and then the contribution from the solvent was removed by subtracting the solvent spectra, corrected using a scaling factor. For the gel, the CH_2 symmetric and antisymmetric stretching vibration bands appear at 2849 cm^{-1} and 2919 cm^{-1}, respectively. These values are smaller than those obtained for $PalG_3H$ in DMSO-d_6 (2855 cm^{-1} and 2926 cm^{-1}), in which $PalG_3H$ is molecularly dispersed, and are comparable with those obtained for a crystalline solid of alkanes having an all-*trans* conformation (2851 cm^{-1} and 2918 cm^{-1}).[19] This indicates that the alkyl chain in the $PalG_3H$ is extended with a near all-*trans* conformation in the gel state. Also, the stretching vibration due to the C=O group in amide moieties is detected at 1645 cm^{-1} and 1632 cm^{-1} for the gel, while that of $PalG_3H$ in DMSO-d_6 only shows at 1670 cm^{-1}, which also included in part the C=O vibration due to trifluoroacetate.[20] The smaller values obtained for the gel relative to that obtained for the DMSO-d_6 solution are characteristic of hydrogen bonding.[21] Thus, it is most likely that the two bands observed in the gel are assignable to the C=O groups, which form weak and strong hydrogen bonding interactions, respectively. Here, it should be noted that there is no significant difference between the FT-IR spectra of the gels and the sol. This observation suggests that the $PalG_3H$ molecules form a fibrous assembly, accompanied by alkyl chain ordering and hydrogen bonding in both the gel and the sol.

Fig. 7 shows the small angle X-ray scattering (SAXS) profiles obtained for (a) the initial gel, (b) the sol obtained by shaking the gel and (c) the gel obtained by aging the sol for 72 h. The gel has a broad scattering peak centered at a scattering vector (q) of approximately 1.0 nm^{-1}. This q value corresponds to a domain spacing (d-spacing) of 6.3 nm. In general, a scattering contrast in SAXS arises from differences in the electron density.[22] The electron density of a peptide moiety is relatively higher than that of an alkyl chain. Therefore, the d-spacing should reflect the distance between the peptide moieties, namely the diameter of the fibrous assembly when the fibrils form bundled structures.[23] Taking into account the FT-IR result that the alkyl chain in $PalG_3H$ is in a *trans* conformation, the length of the $PalG_3H$ molecule can be estimated to be 4.0 nm. The d-spacing observed by SAXS was larger than the molecular length but less than twice that length. These results led us to assume that the $PalG_3H$ molecules form a micelle-like assembly with interdigitated alkyl chains, as shown in the inset of Fig. 7. Such an assembled structure allows the $PalG_3H$ molecules to form hydrogen bonds, consistent with the results obtained in the FT-IR spectroscopic measurements. An important fact here is that there is no substantial difference in the d-spacing reflected in the SAXS profiles of the initial gel, the sol obtained by shaking the gel and the gel obtained by aging the sol for 72 h, although a slight shoulder peak at $q = 1.6$ (d-spacing: 3.9 nm) is observed for the gel obtained by aging the sol. This indicates that the assembled states formed by the $PalG_3H$ molecules in the gel and the sol are comparable. Hence, the molecular assembled state did not change during the sol-to-gel transition even though homogenization of the local environment occurred.

Morphology of the fibrous assembly

To observe the morphology of the fibrous assembly formed by $PalG_3H$ in water, fluorescence microscopy was employed using sodium 8-anilino-1-naphthalenesulfonate (ANS) as a fluorescent probe. The ANS dye is hardly soluble in pure water and provides a stronger fluorescence emission in a hydrophobic environment compared with that in a hydrophilic one.[24] These features make it possible to stain a hydrophobic core in a micelle-like assembly. Before the fluorescence microscopic observations, we measured the fluorescence spectra of the $PalG_3H$–water mixture containing ANS. Fig. 8 shows the fluorescence spectra of ANS in the initial gel and the sol obtained by shaking the gel. Also, the fluorescence spectrum of ANS in water is provided as a reference in the figure. The fluorescence intensity of ANS in the $PalG_3H$–water mixture, regardless of whether it is in the gel or the sol state, is significantly higher than that of the ANS in water. This confirms that the ANS dyes locate in a hydrophobic domain of the $PalG_3H$ assembly. In other words, the $PalG_3H$ molecules form an assembly having a hydrophobic core in the gel and the sol. Importantly, the fluorescence intensity of the ANS in the gel and the sol is comparable. Thus, it can be assumed that the assembled state of

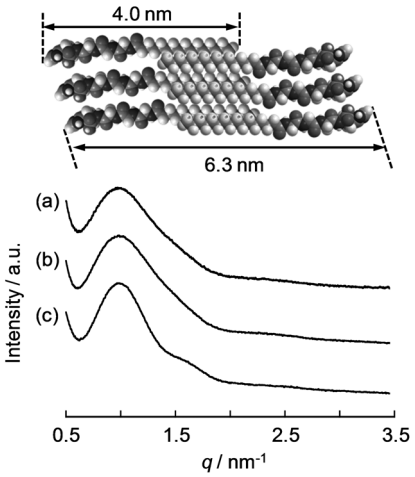

Fig. 7 SAXS profiles of the $PalG_3H$–water mixture (a) as a gel, (b) as a sol at 0 h aging and (c) as a gel at 72 h aging.

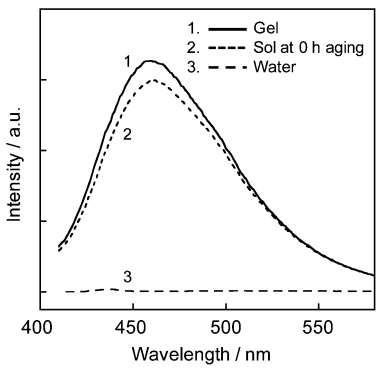

Fig. 8 Fluorescence spectra of ANS in water and the $PalG_3H$–water mixture as a gel and as a sol at 0 h aging. The excitation wavelength ($\lambda_{ex.}$): 380 nm.

$PalG_3H$ is preserved even when the gel is physically shaken to transform into the sol. This is consistent with the results obtained using FT-IR spectroscopic and the SAXS measurements.

Fig. 9 shows the fluorescence microscopic images obtained for the ANS-containing $PalG_3H$ mixture at various stages of the sol-to-gel transition (aging times: 0 h, 12 h and 72 h). Although fibrils with a diameter below 1 μm were observed in both the sol and the gel, their morphology was different depending on the aging time. In the case of the sol at 0 h aging, high and low density regions of fibrils were observed as evidenced by the presence of dark and white regions. Of course, some of the fibrils should be present in a dark region, except that they cannot be observed under the contrast condition used here. As the aging time increased, the dense regions became more interconnected with each other leading to a homogeneous appearance of the network structure at the aging time of 72 h. Invoking that the notion of the network structure based on the fibril entanglements is effective even for SMGs, it is quite reasonable that the $PalG_3H$–water mixture did not flow after aging for 72 h.

Discussion on a possible origin of the heterogeneity

Fluorescence microscopic observations revealed the existence of high and low density regions of fibrils in the sol. In a lower density region, the embedded particles could be expected to be less trapped – and therefore would result in relatively larger $\langle \Delta r^2(\tau) \rangle$ values – as compared to those embedded in the highly dense region. Such an interpretation can be supported by related work conducted by other groups.[25] For instance, a hydrogel based on a F-actin network showed mainly two sets of populations in terms of the behavior of probe particles embedded in it. Some particles become sterically trapped in F-actin rich regions, while other particles move relatively freely in actin-depleted regions. The existence of these two kinds of particle behaviors had been shown to result in a wide and asymmetric $\langle \Delta r^2(\tau) \rangle$ distribution. Therefore, it can be reasonably assumed that the sol state, due to its more heterogeneous network compared to the gel state, provides a heterogeneous microrheological environment for the probe particles, which can correspondingly explain the wide variation in the displacement profiles of the embedded particles.

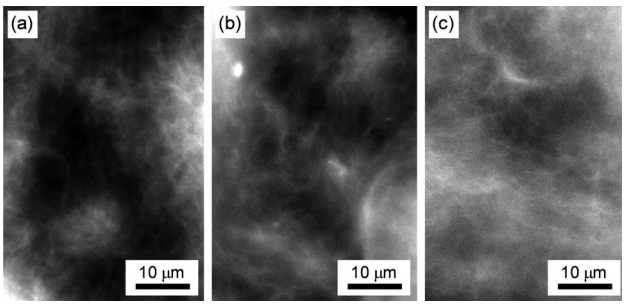

Fig. 9 Fluorescence microscopic images of ANS containing $PalG_3H$–water mixture at various aging times, (a) 0 h, (b) 12 h, and (c) 72 h after physically disrupting the gel.

We also found that the heterogeneity in the fibrous network became less in the course of the sol-to-gel transition, although the assembled state of the $PalG_3H$ molecules in the fibrils did not change. The change in the network can be associated with the variation in the particle displacements in the same manner. Here, we discuss the results obtained by the particle tracking study with larger particles. The particles with a diameter of 3 μm did not provide the wide variation in their displacement profiles seen in the smaller particles regardless of the aging time. This might be because the particle is located in both the higher and lower density regions and thus the particle is insensitive to the difference in the fibril density. Thus, we assume that the size of regions having higher and lower fibril densities is smaller than 3 μm.

Conclusions

We have studied the diffusion behavior of probe particles embedded in a sol obtained by physically disrupting a gel, during the re-gelation process. The particle tracking experiments revealed that the sol was more heterogeneous than the initial gel in terms of its viscoelastic properties and the extent of the heterogeneity decreased as the re-gelation proceeded. The origin of such homogenization was associated with the change in the fibril network, also establishing that this is not related to the assembled state of the $PalG_3H$ molecules, which remains comparable in the gel and sol states. From a particle tracking study using different particle sizes, the characteristic length scale of the heterogeneous network was established to be smaller than 3 μm. The findings of this study should provide a breakthrough concept in understanding and controlling the gelation, leading to the design and functionalization of SMGs.

Acknowledgements

This research was partly supported by a Grant-in-Aid for Scientific Research (B) (no. 24350061) from the Ministry of Education, Culture, Sports, Science and Technology, Japan. The synchrotron radiation facilities experiments were performed at BL40B2 in the SPring8 with the approval of the Japan Synchrotron Radiation Research Institute (JASRI) (Proposals 2011B1624 and 2011A1557).

Notes and references

1 (*a*) J. A. A. W. Elemans, A. E. Rowan and R. J. M. Notle, *J. Mater. Chem.*, 2003, **13**, 2661; (*b*) T. Hashimoto, *Bull. Chem. Soc. Jpn.*, 2005, **78**, 1; (*c*) K. Ariga, Q. Ji, J. P. Hill and A. Vinu, *J. Inorg. Organomet. Polym.*, 2010, **20**, 1; (*d*) H.-B. Yao, H.-Y. Fang, X.-H. Wang and S.-H. Yu, *Chem. Soc. Rev.*, 2011, **40**, 3764.

2 (*a*) S. Mukhopadhyay, U. Maitra, I. G. Krishnamoorthy, J. Schmidt and Y. Talmon, *J. Am. Chem. Soc.*, 2004, **126**, 15905; (*b*) S. K. Kundu, T. Matsunaga, M. Yoshida and M. Shibayama, *J. Phys. Chem. B*, 2008, **112**, 11537; (*c*) Y. Gao, M. J. C. Long, J. Shi, L. Hedstrom and B. Xu, *Chem. Commun.*, 2012, **48**, 8404; (*d*) M. T. Kao, C. Schafer,

G. Raffy and A. Del Guerzo, *Photochem. Photobiol. Sci.*, 2012, **11**, 1730.

3 (*a*) O. Gronwald, E. Snip and S. Shinkai, *Curr. Opin. Colloid Interface Sci.*, 2002, **7**, 148; (*b*) N. M. Sangeetha and U. Maitra, *Chem. Soc. Rev.*, 2005, **34**, 821; (*c*) M. de Loos, J. H. van Esch, R. M. Kellogg and B. L. Feringa, *Tetrahedron*, 2007, **63**, 7285; (*d*) P. Mukhopadhyay, N. Fujita, A. Takada, T. Kishida, M. Shirakawa and S. Shinkai, *Angew. Chem., Int. Ed.*, 2010, **49**, 6338; (*e*) V. A. Mallia, P. Terech and R. G. Weiss, *J. Phys. Chem. B*, 2011, **115**, 12401; (*f*) Y. Liu, T. Wang and M. Liu, *Chem.–Eur. J.*, 2012, **18**, 14650; (*g*) A. Dawn, T. Shiraki, H. Ichikawa, A. Takada, Y. Takahashi, Y. Tsuchiya, L. T. N. Lien and S. Shinkai, *J. Am. Chem. Soc.*, 2012, **134**, 2161.

4 (*a*) M. Shirakawa, N. Fujita and S. Shinkai, *J. Am. Chem. Soc.*, 2005, **127**, 4164; (*b*) T. Shirosaki, S. Chowdhury, M. Takafuji, D. Alekperov, G. Popova, H. Hachisako and H. Ihara, *J. Mater. Res.*, 2006, **21**, 1274; (*c*) X. Huang, S. R. Raghavan, P. Terech and R. G. Weiss, *J. Am. Chem. Soc.*, 2006, **128**, 15341; (*d*) A. Shundo, K. Mizuguchi, M. Miyamoto, M. Goto and K. Tanaka, *Chem. Commun.*, 2011, **47**, 8844; (*e*) T. D. Hamilton, D. K. Bucar, J. Baltrusaitis, D. R. Flanagan, Y. Li, S. Ghorai, A. V. Tivanski and L. R. MacGillivray, *J. Am. Chem. Soc.*, 2011, **133**, 3365; (*f*) G. O. Lloyd, M.-O. M. Piepenbrock, J. A. Foster, N. Clarke and J. W. Steed, *Soft Matter*, 2012, **8**, 204.

5 (*a*) I. W. Hamley, *Soft Matter*, 2011, **7**, 4122; (*b*) M. Guvendiren, H. D. Lu and J. A. Burdick, *Soft Matter*, 2012, **8**, 260.

6 (*a*) A. Ashkin, *Proc. Natl. Acad. Sci. U. S. A.*, 1997, **94**, 4853; (*b*) T. G. Mason, K. Ganesan, J. H. van Zanten, D. Wirtz and S. C. Kuo, *Phys. Rev. Lett.*, 1997, **79**, 3282; (*c*) J. Liu, M. L. Gardel, K. Kroy, E. Frey, B. D. Hoffman, J. C. Crocker, A. R. Bausch and D. A. Weitz, *Phys. Rev. Lett.*, 2006, **96**, 118104; (*d*) F. K. Oppong and J. R. de Bruyn, *J. Non-Newtonian Fluid Mech.*, 2007, **142**, 104; (*e*) G. Pesce, A. C. De Luca, G. Rusciano, P. A. Netti, S. Fusco and A. Sasso, *J. Opt. A: Pure Appl. Opt.*, 2009, **11**, 034016; (*f*) K. Hori, D. P. Penaloza, A. Shundo and K. Tanaka, *Soft Matter*, 2012, **8**, 7361; (*g*) A. Shundo, K. Hori, D. P. Penaloza and K. Tanaka, *Rev. Sci. Instrum.*, 2013, **84**, 014103.

7 K. M. Schultz and E. M. Furst, *Soft Matter*, 2012, **8**, 6198.

8 (*a*) M. T. Valentine, P. D. Kaplan, D. Thota, J. C. Crocker, T. Gisler, R. K. Prudhomme, M. Beck and D. A. Weitz, *Phys. Rev. E: Stat., Nonlinear, Soft Matter Phys.*, 2001, **64**, 061506; (*b*) Y. Tseng, K. M. An and D. Wirtz, *J. Biol. Chem.*, 2002, **277**, 18143; (*c*) A. Aufderhorst-Roberts, W. J. Frith and A. M. Donald, *Soft Matter*, 2012, **8**, 5940; (*d*) D. P. Penaloza, K. Hori, A. Shundo and K. Tanaka, *Phys. Chem. Chem. Phys.*, 2012, **14**, 5247.

9 D. Koda, T. Maruyama, N. Minakuchi, K. Nakashima and M. Goto, *Chem. Commun.*, 2010, **46**, 979.

10 (*a*) C. Finder, M. Wohlgemuth and C. Mayer, *Part. Part. Syst. Charact.*, 2004, **21**, 372; (*b*) B. R. Long and T. Q. Vu, *Biophys. J.*, 2010, **98**, 1712.

11 F. K. Oppong, P. Coussot and J. R. de Bruyn, *Phys. Rev. E: Stat., Nonlinear, Soft Matter Phys.*, 2008, **78**, 021405.

12 (*a*) F. Amblard, A. C. Maggs, B. Yurke, A. N. Pargellis and S. Leibler, *Phys. Rev. Lett.*, 1996, **77**, 4470; (*b*) A. Palmer, T. G. Mason, J. Xu, S. C. Kuo and D. Wirtz, *Biophys. J.*, 1999, **76**, 1063; (*c*) I. Y. Wong, M. L. Gardel, D. R. Reichman, E. R. Weeks, M. T. Valentine, A. R. Bausch and D. A. Weitz, *Phys. Rev. Lett.*, 2004, **92**, 178101.

13 (*a*) H. Qian, M. P. Sheetz and E. L. Elson, *Biophys. J.*, 1991, **60**, 910; (*b*) C. Oelschlaeger, N. Willenbacher and S. Neser, in *Surface and Interfacial Forces – From Fundamentals to Applications*, ed. G. Auernhammer, H.-J. Butt and D. Vollmer, Springer, Heidelberg, 2008, pp. 74–79.

14 H. A. Houghton, A. I. Hasnain and A. M. Donald, *Eur. Phys. J. E*, 2008, **25**, 119.

15 W. K. Kegel and A. van Blaaderen, *Science*, 2000, **287**, 290.

16 (*a*) A. Rahman, *Phys. Rev.*, 1964, **136**, A405; (*b*) N. Yamamoto, M. Ichikawa and Y. Kimura, *Phys. Rev. E: Stat., Nonlinear, Soft Matter Phys.*, 2010, **82**, 021506.

17 T. Moschakis, A. Lazaridou and C. G. Biliaderis, *J. Colloid Interface Sci.*, 2012, **375**, 50.

18 (*a*) M. T. Valentine, Z. E. Perlman, M. L. Gardel, J. H. Shin, P. Matsudaira, T. J. Mitchison and D. A. Weitz, *Biophys. J.*, 2004, **86**, 4004; (*b*) S. Matsumoto, S. Yamaguchi, S. Ueno, H. Komatsu, M. Ikeda, K. Ishizuka, Y. Iko, K. V. Tabata, H. Aoki, S. Ito, H. Noji and I. Hamachi, *Chem.–Eur. J.*, 2008, **14**, 3977.

19 (*a*) R. A. MacPhail, H. L. Strauss, R. G. Snyder and C. A. Elliger, *J. Phys. Chem.*, 1984, **88**, 334; (*b*) N. V. Venkataraman and S. Vasudevan, *J. Phys. Chem. B*, 2001, **105**, 1805.

20 L. E. Valenti, M. B. Paci, C. P. De Pauli and C. E. Giacomelli, *Anal. Biochem.*, 2011, **410**, 118.

21 (*a*) N. Yamada, K. Ariga, M. Naito, K. Matsubara and E. Koyama, *J. Am. Chem. Soc.*, 1998, **120**, 12192; (*b*) J. P. Schneider, D. J. Pochan, B. Ozbas, K. Rajagopal, L. Pakstis and J. Kretsinger, *J. Am. Chem. Soc.*, 2002, **124**, 15030.

22 O. Glatter, in *Small-Angle X-ray Scattering*, ed. O. Glatter and O. Kratky, Academic Press, London, 1982.

23 (*a*) K. Sakurai, Y. Jeong, K. Koumoto, A. Friggeri, O. Gronwald, S. Sakurai, S. Okamoto, K. Inoue and S. Shinkai, *Langmuir*, 2003, **19**, 8211; (*b*) Y. Jeong, A. Friggeri, I. Akiba, H. Masunaga, K. Sakurai, S. Sakurai, S. Okamoto, K. Inoue and S. Shinkai, *J. Colloid Interface Sci.*, 2005, **283**, 113; (*c*) P. Duan, L. Qin, X. Zhu and M. Liu, *Chem.–Eur. J.*, 2011, **17**, 6389.

24 (*a*) L. Stryer, *J. Mol. Biol.*, 1965, **13**, 482; (*b*) M. Suzuki, M. Yumoto, M. Kimura, H. Shirai and K. Hanabusa, *Helv. Chim. Acta*, 2004, **87**, 1; (*c*) S. Kiyonaka, K. Sada, I. Yoshimura, S. Shinkai, N. Kato and I. Hamachi, *Nat. Mater.*, 2004, **3**, 58.

25 J. Apgar, Y. Tseng, E. Fedorov, M. B. Herwig, S. C. Almo and D. Wirtz, *Biophys. J.*, 2000, **79**, 1095.

